http://dx.doi.org/10.5012/bkcs.2013.34.4.1089

Overexpression and Biological Characterization of the Death Domain Complex between TRADD and FADD

Eun Young Hwang,[a] Mi Suk Jeong,[a] Minkyung Sung,[a] and Se Bok Jang[*]

Department of Molecular Biology, College of Natural Sciences, Pusan National University, Busan 609-735, Korea
[*]E-mail: sbjang@pusan.ac.kr
Received November 15, 2012, Accepted January 14, 2013

The tumor necrosis factor-receptor 1 (TNFR1)-associated death domain protein (TRADD) contains an N-terminal TRAF binding domain and a C-terminal death domain. TRADD is known to interact directly with TNF receptor 2 (TNFR2) and the Fas-associated death domain protein (FADD), which are signal transducers that activate NF-kB and induce apoptosis, respectively. To date, there has been no structural information on the TRADD and FADD death domain (DDs) complex. In this study, the death domains of TRADD and FADD were co-expressed and purified from *Escherichia coli* for structural characterization. We found that human TRADD (hTRADD) interacted strongly with mouse FADD (mFADD) *via* their DDs and interacted weakly with human FADD (hFADD)-DD. Moreover, the structures of the TRADD-DD:FADD-DD complexes were separately modeled from predicted structures in the protein data bank (PDB). The results of this study will have important applications in human diseases such as cancer, AIDS, degenerative and autoimmune diseases, and infectious diseases.

Key Words : Soluble expression, TRADD, FADD, Interaction

Introduction

The TRADD adaptor protein is a multifunctional protein that is recruited to TNFR1 upon ligand binding. TRADD contains two separate domains, allowing it to bind to several protein partners and participate in different signaling pathways.[1] The C-terminal of TRADD contains a DD, which is a central component in cell death signaling after TNFR1 stimulation. The death domain superfamily is the prime mediator of interactions necessary for apoptosis, innate immunity and the necrosis signaling pathway.[2] Death domains now appear to define the interaction domains that are capable of both homotypic and heterotypic associations.[3-5] These observations suggest that death domains may function as adaptors to couple some members of the TNFR superfamily (at least TNFR1 and Fas) to other signaling proteins.

The TRADD death domain has the ability to auto-aggregate and bind to the death domains of the pro-apoptotic FADD and the serine-threonine kinase receptor-interacting protein 1 (RIP1).[6] TRADD can recruit FADD and promote Caspase-8 activation and apoptosis through an extrinsic pathway. FADD couples the TNFR1-TRADD complex to the activation of Caspase-8, which initiates apoptosis.[7] In TNF-treated cells, TNFR1, TRADD, FADD, and RIP kinase proteins form signaling complexes *via* modular interaction within their C-terminal death domains.[8] Structural information regarding DDs and their interactions with partners will provide a molecular basis for assembly of DD mediated complexes and regulation of apoptosis and the innate immune signaling pathway.

To date, no structural information pertaining to the TRADD and FADD death domain (DDs) complexes has been available. In this study, the death domains of TRADD and FADD were co-expressed and purified from *E. coli* for structural characterization. We then predicted the 3D structure of the TRADD-DD:FADD-DD complex using the SWISS-MODEL software, which has been used for homology-based protein structure modeling. In addition, the interactions of TRADD with human FADD and mouse FADD were compared by structural modeling. Structural prediction will be an important research topic in bioinformatics and have important applications in medicine and other fields, such as drug design and disease prediction.

Materials and Methods

Cloning and Expression. The construct for the expression of human TRADD-DD (160-308) was made as follows. Full-length hTRADD was used as a template for PCR and plasmid vector pET26b was used to add a hexahistidine tag at the carboxy-terminus of TRADD-DD for affinity purification. PCR products were then digested with *Nde*I and *BamH*I restriction enzymes and ligated into pET26b. For co-expression of the TRADD-DD:FADD-DD complex, hFADD-DD (93-184) was first digested with the *Nhe*I and *BamH*I restriction enzymes and then ligated into pET28a. The portion of the T7 promoter containing the ribosome-binding site (RBS) and the coding region of the TRADD-DD was subsequently amplified by PCR using oligonucleotides containing the *BamH*I and *Hind*III restriction sites. The amplified region of the pET26b containing TRADD-DD was incorporated into the downstream portion of the pET28a that already

[a]These authors contributed equally to this work.

contained the coding region of the FADD-DD. This co-expression construct included a single promoter with two different genes, each one preceded by its own RBS. Single or double mutations of hFADD were used for the complex structural analysis. Specifically, a deletion mutation (R184) of hFADD-DD was performed. Two polar amino acids (Q182 and N102) were mutated to negatively charged amino acids (E182 and D102) *via* site-specific mutagenesis using the PCR technique.

Expression plasmids of the TRADD-DD alone and TRADD-DD:FADD-DD complex were identified by restriction endonuclease digestion and further verified by DNA sequencing on a Macrogen automatic DNA sequencer. The constructs were transformed into the expression host *Escherichia coli* BL21(DE3). Briefly, a single colony was inoculated into 20 mL of Luria-Bertani (LB) medium containing 50 mg/mL of ampicillin and cultured overnight at 37 °C. These cells were then added to 500 mL of LB medium containing 10 μg/mL of kanamycin and cultivated at 37 °C until an OD_{600} of 0.5 was reached. The expression of these proteins was then induced by the addition of 0.5 mM isopropyl-thio-β-D-galactopy ranoside (IPTG) for six hours at 25 °C, after which cells were harvested by centrifugation at 4,600 rpm for 25 min. The cell pellets were then either immediately used or stored at −70 °C. Next, the TRADD-DD alone and DDs complex cell pellets were resuspended in lysis buffer A [50 mM Tris-HCl (pH7.5), 200 mM NaCl, and 1 mM dithiothreitol (DTT)] and sonicated on ice (Branson Sonifier 450), after which the cell lysates were centrifuged at 13,500 rpm for 45 min to remove the insoluble cellular debris.

Purification. His-tagged fusion proteins of the TRADD-DD:FADD-DD complex were applied to a Ni-NTA (Amersham Pharmacia Biotech) column for purification. The supernatant obtained from the protein extraction step was then loaded onto a Ni-NTA column that had been pre-equilibrated with buffer A. All buffers were passed through a 0.45-μm Minisart membrane filter prior to use. The column was then washed with buffer A containing imidazole, after which the bound protein was eluted by varying the concentration of imidazole from 20 mM to 200 mM. Protein elution was monitored at 280 nm, and the resulting fractions were analyzed by 15% SDS-PAGE. Gel filtration was then performed using a fast protein liquid chromatography (FPLC) system equipped with a Superdex 200 10/300 GL column. The proteins were loaded onto a column equilibrated with buffer A and separated at a flow rate of 1.5 mL/min. To obtain more soluble and stable hTRADD-DD protein for evaluation of the biophysical properties, a refolding process was performed. To accomplish this, the inclusion bodies of the hTRADD-DD were re-suspended under various pH conditions in buffer A and then centrifuged at 13,500 rpm for 45 min at 4 °C, after which the supernatant was collected and loaded onto a column containing pre-equilibrated Ni-NTA resin. Gel filtration was then performed using a FPLC system equipped with a Superdex column. The purity of purified hTRADD-DD was determined by SDS-PAGE gel.

UV-Vis Absorption. Absorbance was measured using a Shimadzu UV-1650 PC UV-Vis spectrophotometer with 1.0 cm quartz cells. The UV absorbance spectra of the hTRADD-DD were obtained using concentrations of 0.5 mg/mL. pH-dependent unfolding studies were carried out under various pH values (pH 7.5-10.5). The UV spectra of the hTRADD-DD were recorded in the 285-310 nm range.

Fluorescence Spectroscopy. Fluorescence emission spectra were obtained using an Edinburgh (UK) FLS920 Time Correlated Single Photon Counting Spectrometer (TCSPC) with 1 cm path length cuvettes containing excitation and emission slits 20 nm in width. The fluorescence emission spectra of TRADD and FADD were obtained to identify characteristic chemical structures, namely double bonds and aromatic groups. The emission intensity was recorded at 300-460 nm with an excitation wavelength of 295 nm. hTRADD-DD and hFADD-DD:mFADD-DD at a concentration of 5 μM were preincubated together for 25 min at 25 °C. All spectra were obtained at a protein concentration of 50 μg/mL. Ten spectra from each protein sample were collected, averaged, and subjected to baseline correction by subtracting the buffer spectrum.

GST Pull Down Assay. For the pull-down assay, 50 μg purified GST-tagged TRADD or control protein (GST) was mixed with 50 μg purified His-tagged mouse FADD or human FADD, respectively. Then, glutathione sepharose 4B beads were added in Tris buffer [50 mM Tris-HCl (pH 7.5) and 200 mM NaCl] by rotating at 4 °C for 2 h. By centrifuging at 3,000 rpm for 5 min, the supernatant was removed, and the beads were washed four times with wash buffer [50 mM Tris-HCl (pH 7.5) and 200 mM NaCl]. For each time, the beads were incubated with the wash buffer on rotator for 10 min and collected by centrifuging at 3,000 rpm for 2 min. Proteins bound to the beads were eluted with buffer [50 mM Tris-HCl (pH 7.5) and 30 mM glutathione], and resolved on 15% SDS polyacrylamide gel. The proteins were analyzed by Western blot.

Western Blot Analysis. Proteins resolved on 15% SDS polyacrylamide gel were transferred onto polyvinylidene difluoride (PVDF) membrane (Millipore). The membrane was blocked for 12 h with 5% skim milk in PBS-T (1X PBS, 0.1% tween 20). After incubating with anti-His (Santa Cruz Biotech) or anti-GST (Santa Cruz Biotech) diluted to 1:5000 for 1 h, the membrane was rinsed three times with PBS-T (1X PBS, 0.1% tween 20) for 10 min and incubated with appropriate horseradish peroxidase (HRP) conjugated secondary antibodies (Santa Cruz Biotech) diluted to 1:10,000 for 80 min. The proteins were detected using Chemiluminescent Sensitive Luminol-Reagent A (Surmodics) after three times rinse with PBS-T.

3D Structural Prediction of TRADD and FADD-DDs. Models of the TRADD-DD and FADD-DD were constructed using the SWISS-MODEL software, which has previously been used for relative protein structure modeling.[10] The results of an Expert Protein Analysis System (EXPASY) search with the PDB revealed three reference proteins with considerable sequence identity, hFADD-DD (PDB ID: 2GF5, 1-191, F25Y), hFADD-DD (PDB ID: 3EZQ, 93-208), and

Table 1. Ramachandran analysis

	hTRADD-DD	hFADD-DD	mFADD-DD	hTRADD:mFADD
Most favored Regions (%)	82.2	85.1	89.4	85.5
Additional allowed Regions (%)	18.8	14.9	7.1	12.7
Generously allowed Regions (%)	0.0	0.0	1.2	0.6
Disallowed regions (%)	0.0	1.3	2.4	1.2

mFADD-DD (PDB ID: 1FAD, 89-183, D96Y). The predicted 3D model structures of the TRADD-DD:FADD-DD complex were aligned and the structurally conserved regions (SCRs) of the model and template were determined by superposition of the two structures and multiple sequence alignments generated by CLUSTAL W.

Root Mean Square Comparisons of the Backbone Fold. Based on the carbons (Cα), the root mean square (rms) deviations of the hFADD-DD and mFADD-DD models were calculated from the PDB structure using the SPDBV application (Swiss PDB viewer).[9] As shown in Figure 3(c), the average deviations in rms were generally within 1.25 Å, which further confirmed the reliability of the predicted model. The model was built using a considerable number of template structures, and most parameters were highly correlated throughout the study.

Secondary Structure Prediction. The secondary structure was predicted using the Jalview program, which uses 3D coordinates from PDB files to calculate the secondary structure and local environmental features and displays the same in a color-coded format in the sequence alignment.

Ramachandran Analysis of TRADD Alone and the TRADD-DD:FADD-DD Complex. The model was analyzed based on Ramachandran plot calculations computed using the PROCHECK program.[10] PROCHECK compares residue orientations in the model to those permitted by Ramachandran plots, chi-chi^2 plots, main and side chain torsions, and residue properties. The φ and ψ distributions of the Ramachandran plots of nonglycine and non-proline residues were observed. PROCHECK analysis indicated that all models showed adequate stereochemistry, with nearly 100% of the amino acid side chains being located in allowed regions of the Ramachandran plot (Table 1).

Results and Discussion

Full-length TRADD (1-312) contains an N-terminal domain (51-144) and C-terminal death domain (215-304) (Fig. 1(a)). TRADD interacts with TRAF2 through its N-terminal domain and with FADD through its C-terminal death domain.[7] Full-length FADD (1-208) contains both an N-terminal DED (3-84) and a C-terminal DD (93-184) and interacts with FLIP and TRADD through DED-DED and DD-DD, respectively.

To date, there has been no information pertaining to the three-dimensional structure of the TRADD-DD:FADD-DD complex available. In this study, hTRADD-DD alone was expressed in *E. coli* in an insoluble form (Fig. 1(b)). About 30% hydrophobic amino acids (17L, 6A, 4V, 2F, and 1P) were observed in hTRADD-DD. The hydrophobic amino acids in DD may cause aggregation. FADD-DD was overexpressed in a soluble form. To obtain a soluble TRADD-DD:FADD-DD complex, we constructed five different co-expression systems using TRADD-DD and FADD-DD (Fig. 1(c)-(g)). We successfully expressed high soluble levels of His-tagged TRADD-DD:FADD-DD complexes in *E. coli*. Overexpressed His-tagged complexes were identified in the supernatant of the large-scale culture and had the expected molecular mass of 20 kDa (TRADD-DD) and 15 kDa (FADD-DD), respectively (Fig. 1(c)-(g)). Recently, the crystal structure of the MyD88-DD:IRAK4-DD:IRAK2-DD ternary complex was elucidated.[11] Although all DDs exhibit a six-helix bundles fold, variations have been detected in the direction and length of the helices. These different features may be responsible for their ability to interact with their own partner.[12,13] In this study, the FADD and TRADD complex band from the gel-filtration showed the formation of high oligomeric DD complex (Fig. 2(a)).

Among the five co-expression systems tested, the hTRADD-DD:mFADD-DD complex showed the highest solubility and strongest interaction (Fig. 1(c)). The final concentration of the soluble protein was determined to be 3 mg/mL for the hTRADD-DD:mFADD-DD complex. In contrast, the complexes of hTRADD-DD:hFADD-DD were initially overexpressed, but TRADD-DD gradually disappeared. hTRADD was weakly bound to hFADD-DD and the hTRADD-DD:hFADD-DD complexes showed low solubility during purification (Fig. 1(d)-(g)). The interactions between the hTRADD-DD and hFADD-DD were weak, and both readily dissociated and aggregated.

To confirm the differences of solubility and interaction of hFADD-DD and mFADD-DD to hTRADD-DD, we predicted structures and interactions of hTRADD-DD and FADD-DD. We first predicted a structure of hTRADD-DD based on the hFADD-DD (1-191, F25Y, PDB ID: 2GF5) structure (Fig. 2(b)). The DD structure of hTRADD and hFADD were shown to have similar folding patterns, although their sequence identity was only 27%. The hTRADD-DD possesses a helix-turn-helix (HTH) motif and is composed of six α-helices connected by short or long loops. Nine positive Arg residues in hTRADD-DD were in the pocket. The Arg residues distributed in the secondary structure were densely gathered and created a positive pocket to interact with the FADD-DD. The Arg residues in the hTRADD-DD were located at 2-5 α-helices in the interaction core. In addition, the Arg residues in the loops among the 2-5 α-helices may contribute to the conformational changes and serve as the interacting gate for the negative binding pocket in the FADD-DD structure.

Next, the structure of mFADD-DD (93-183) was predicted using the known structure of mutant mFADD (89-183, D96Y, PDB ID: 1FAD). The death domain of mFADD was approximately 60% identical to that of hFADD. Most of the

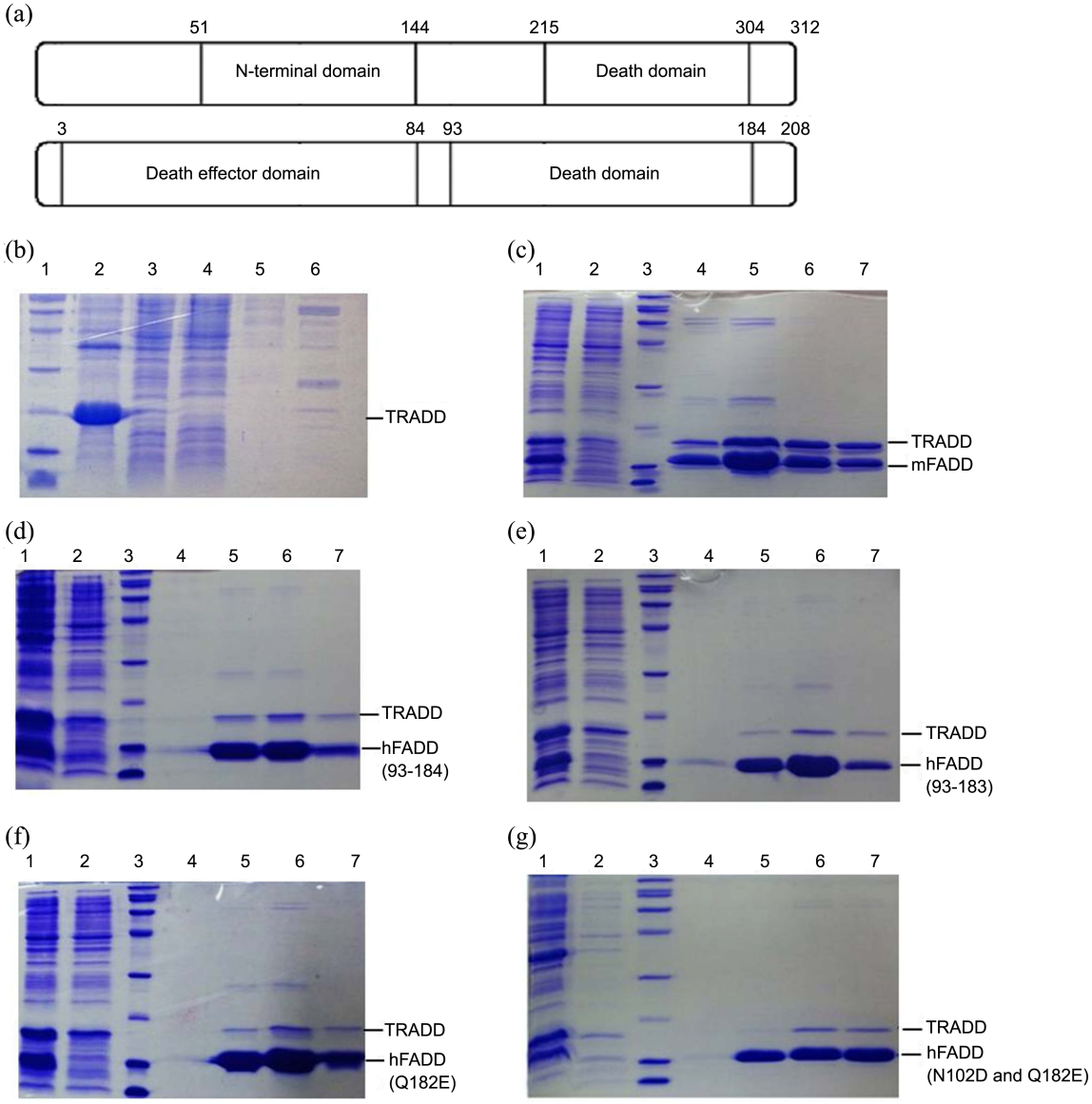

Figure 1. (a) Schematic diagram showing the domains of TRADD (1-312) and FADD (1-208). (b-g) SDS-PAGE analysis of the expressed and purified proteins. (b) Fractions of His-tagged hTRADD-DD (160-308). Lane 1: protein size marker; lane 2: pellet after induction by IPTG; lane 3: supernatant after induction by IPTG; lane 4: unbound fraction; lane 5: washed fraction with 20 mM imidazole; lane 6: eluted fraction with 200 mM imidazole. (c) Co-expression of hTRADD-DD (160-308) and mFADD-DD (93-184) (d) hTRADD-DD and hFADD-DD (93-184) (e) hTRADD-DD and hFADD-DD (93-183) (f) hTRADD-DD and hFADD-DD (Q182E) (g) hTRADD-DD and hFADD-DD (N102D and Q182E). (c-g) Lane 1: supernatant after induction by IPTG; lane 2: unbound fraction; lane 3: protein size marker; lanes 4-7: fractions eluted with 200 mM imidazole.

negative charges in the mFADD-DD were densely packed in the binding pocket (Fig. 2(c)). The negatively charged pocket of the mFADD-DD binds strongly to the positively charged pocket of hTRADD-DD. Because DDs are protein interaction modules, their surface features dictate their mode of interactions with their partners. The difference in the electrostatic surface is critical to interactions with partner proteins.

To compare the binding properties of the hFADD-DD (93-184), we modeled four different hFADD-DD using the hFADD (93-208, 3EZQ). The distribution of negative charges in hFADD-DD (93-184) was less than the distribution of negative changes in mFADD-DD (93-183) (Fig. 2(d)). The R184 positive residue in the hFADD-DD was located at the interface of hTRADD and hFADD. This positive residue may interfere with the interaction between hTRADD-DD and hFADD-DD through a repulsive force. We deleted the R184 residue but the negative charges on the surface of the hFADD-DD (93-183) were still less than those of mFADD-DD. To make the amino acids environment similar to mFADD-DD, the positively charged Q182 residue in hFADD-DD was mutated to E182, or which was negatively charged. The surface of the modeled hFADD-DD (93-183, Q182E) was more negatively charged than that of hFADD-DD (93-183); however, a strong interaction between their DDs was still not

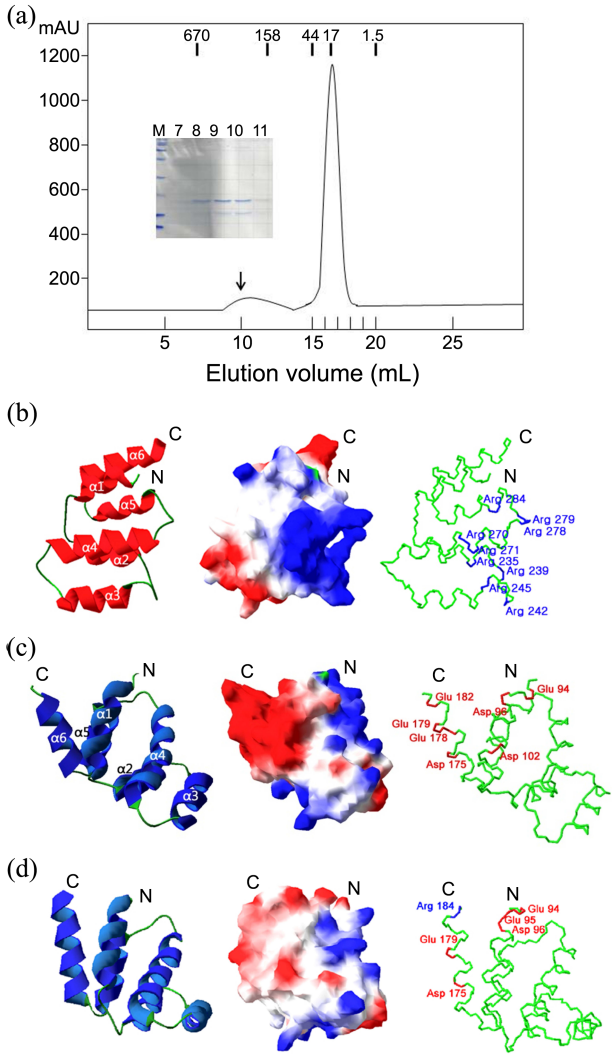

Figure 2. (a) Gel-filtration chromatography of hTRADD:mFADD complex. (b) The predicted structures of hTRADD-DD are shown as a ribbon representation (left panel), surface representation (middle panel), and Cα trace representation (right panel) (c) The mFADD-DD (93-183) is modeled. (d) The hFADD-DD is modeled. The relative distribution of surface charge is shown with acidic regions in red, basic regions in blue and neutral regions in white.

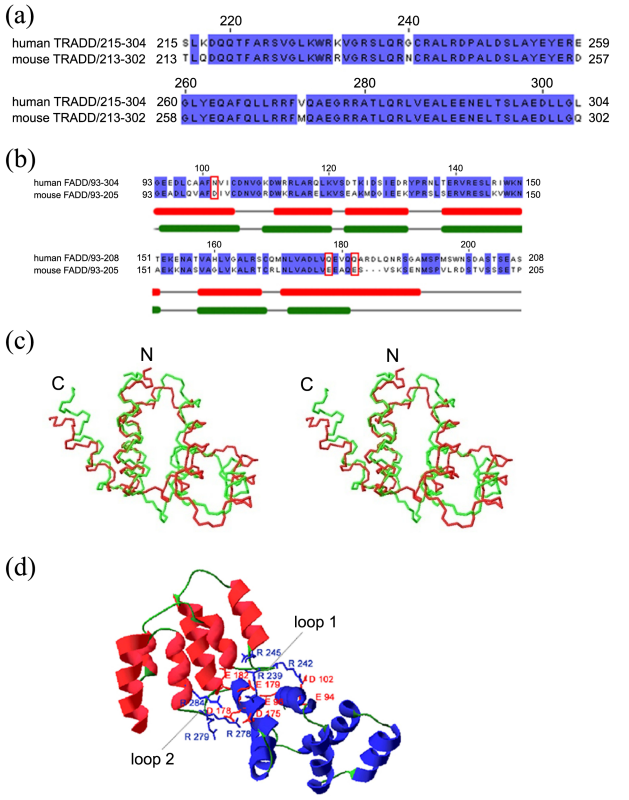

Figure 3. (a) Amino acid sequences of the hTRADD-DD and mTRADD-DD are aligned. (b) The amino acid sequences of the hFADD-DD and mFADD-DD are shown. Sequence alignment of FADD domains and predicted secondary structure of FADD are shown. α-Helices are shown as red ellipses and loops as purple lines. There are no β-sheets. The residues conserved across two species are colored in blue. Mutated residues are indicated by red boxes. (c) Superposition of Cα traces of the mFADD-DD (red) and the hFADD-DD (green). (d) The interactions between hTRADD-DD and mFADD-DD (93-184) were modeled.

observed. In addition, we made double mutations (N102D and Q182E) in hFADD-DD. The surface of the double mutants was very similar to mFADD-DD but it was still not enough to induce a strong interaction. In these experiments, the four different hFADD-DD constructs produced different levels of expression solubility and properties when compared to mFADD-DD (Fig. 1(c)-(g)). We found that the predicted interaction in the structural modeling could play an important role in the structural stability or expression of the protein complex.

TRADD is an evolutionarily highly conserved protein in eukaryotic organisms. The hTRADD and mTRADD proteins showed extensive sequence similarity in their death domains (91%) (Fig. 3(a)). Because the hTRADD and mTRADD proteins have a high sequence similarity, they may have similar interactions with partner proteins. The death domains are completely conserved in hTRADD-DD and mTRADD-DD, with the exception of seven amino acids (S215, K217, K232, G240, E259, V273, and L304). Conversely, the hFADD-DD was not highly conserved relative to mFADD-DD (60%). The secondary structures of the hFADD-DD and mFADD-DD were predicted to be composed of six α-helices (Fig. 3(b)). Interestingly, the sixth α-helix in the hFADD-DD was longer than the other five α-helices in the mFADD-DD. The modeled rms deviation between the mFADD-DD (aa 93-183) and hFADD-DD (aa 93-184) was 1.56 Å (Fig. 3(c)). Superposition of the two structures revealed that residues with rms deviations exceeding about 3.0 Å were located at the connecting loop regions in the core region. These results indicate that conformational changes occurred at the flexible loop regions.

In the hTRADD-DD:mFADD-DD complex, a structural interaction was observed in the loop1 and loop2 regions (R239, R242, R245, R278, R279, and R284) of hTRADD-DD. Moreover, a structural interaction was observed in the regions of the mFADD-DD (E94, E96, D102, D175, D178, E179, and E182) (Fig. 3(d)). The interaction between

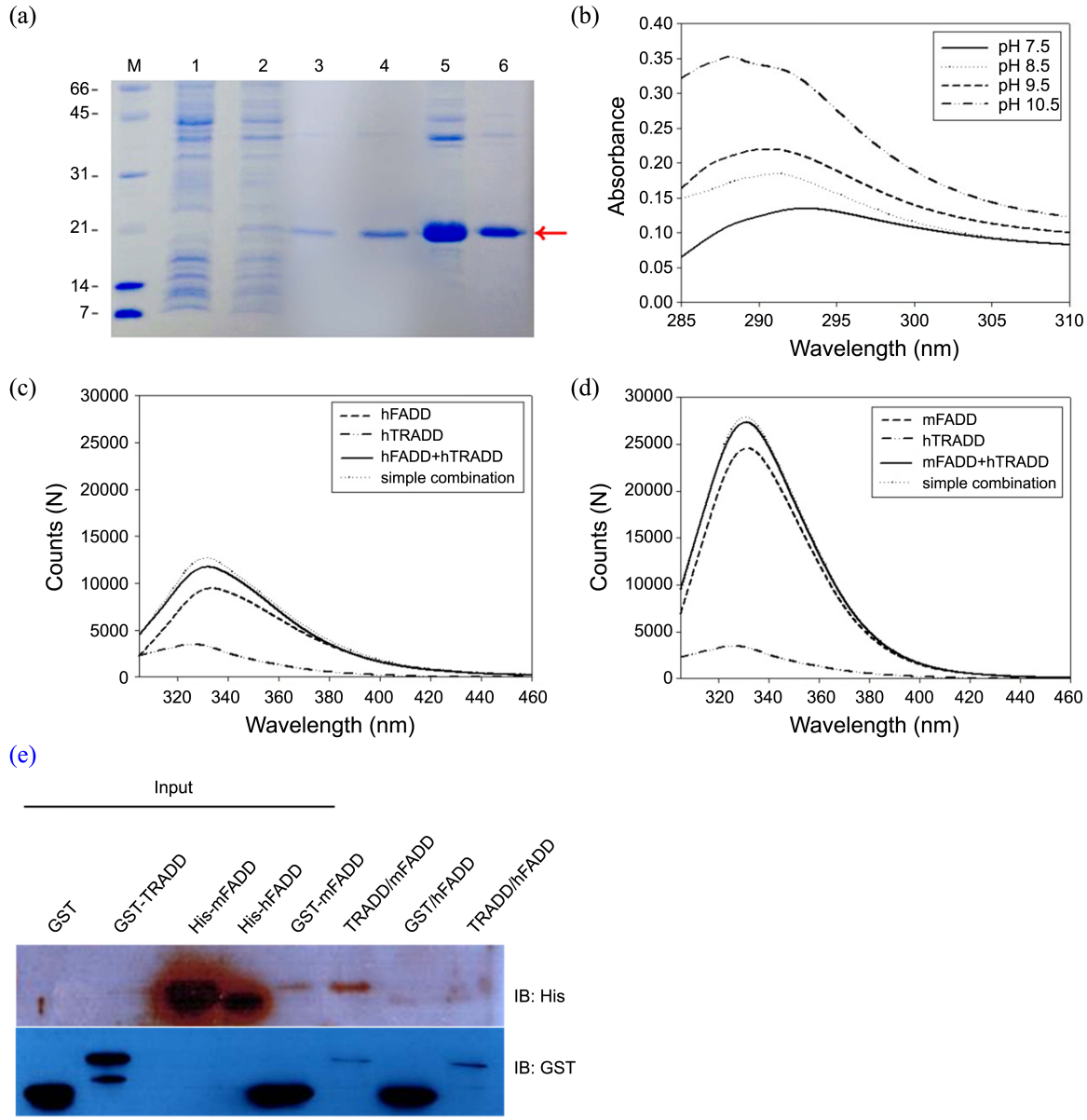

Figure 4. (a) The solubility of hTRADD is sensitive to pH. M: protein size marker; lane 1: 50 mM Tris (pH 7.5); lane 2: Tris (pH 8.5); lane 3: Tris (pH 9.5); lane 4: Tris (pH 10.5); lane 5: Glycine (pH 9.5); lane 6: Glycine (pH 10.5). (b) Soluble hTRADD-DD obtained under various pHs were measured by UV-Vis spectrophotometry. The absorbance was monitored in the 285-310 nm range under various pHs. (c and d) Fluorescence analysis of hTRADD-DD binding to hFADD-DD/mFADD-DD. Fluorescence spectra of the hTRADD-hFADD/mFADD complex and of each individual protein are shown. (e) Analysis of hTRADD-DD binding to hFADD-DD/mFADD-DD by *in vitro* GST-tag pull-down assay.

hTRADD-DD and mFADD-DD was mediated by charged amino acids in the DDs. TRADD-DD contained basic charged amino acids, whereas FADD-DD contained acidic charged amino acids. In the structure of hTRADD-DD, a loop was present in the linker region of the α-helices. A loop region is often flexible and able to adopt several different conformations and accommodate significant structural interactions, expose hydrophobic amino acids, and cause aggregation. PROCHECK analysis indicated that all models showed adequate stereochemistry, with nearly 100% of the amino acid side chains being located in allowed regions of the Ramachandran plot (Table 1).

We also found that solubility of hTRADD-DD is sensitive to various pH values. Specifically, hTRADD-DD showed greater solubility under high pH conditions. The expression of hTRADD-DD was increased at pH 9.5-10.5 (Fig. 4(a)). However, at extremely high pH (9.5-10.5), hTRADD-DD tends to be soluble, but is able to easily aggregate. The conformational changes in hTRADD-DD were also dependent on pH (Figs. 4(a) and (b)). Specifically, UV-Vis absorbance spectroscopy revealed large structural changes at pH values greater than 9.5.

To investigate the interaction between hTRADD-DD and hFADD-DD:mFADD-DD, the fluorescence emission spectra

of purified hTRADD-DD and hFADD-DD:mFADD-DD were measured. The λ_{max} curve was detected at 330 nm (Figs. 4(c) and (d)). The spectrum of the hTRADD-DD:mFADD-DD complex at 335 nm was much higher than that of the hTRADD-DD:hFADD-DD complex. For the hTRADD-DD:hFADD-DD/mFADD-DD complex, the fluorescence intensities were approximately 3,000 N for hTRADD-DD, 9,000 N for hFADD-DD, and 24,000 N for mFADD-DD. Both spectra of the hTRADD-DD:hFADD-DD/mFADD-DD complex were slightly lower than those obtained when hTRADD-DD: hFADD-DD/mFADD-DD were simply combined. To further determine whether hTRADD-DD interacts with hFADD-DD or mFADD-DD, GST pull down assays were performed. From detected protein bands, we assumed that hTRADD interacts more strongly with mFADD-DD than hFADD-DD (Fig. 4(e)).

Expression and crystallization of the full-length TRADD and FADD complex have proven to be difficult. There are currently no crystal or solution structures available for the full-length TRADD. The available structural information is derived from the structures of fragments or domains of the protein or inferred by homology modeling from partial structures of other FADD members. The 3D structure of the death domain of TRADD (215-304) predicted by homology modeling is similar to that of hFADD (1-191, PDB ID: F25Y), which consists of 6 α-helices. In the FADD-DD, most residues of the binding region have negative charges, while most residues of the binding region in TRADD-DD have positive charges in the globular fold. The loop region is composed of a flexible linker structure and DD regions that are in close contact to stabilize their charges. The results of this study will help elucidate the role of the DDs of TRADD and FADD in apoptosis signal transduction. In addition, the predicted TRADD-DD and FADD-DD complex structure may prove to be an important target in the development of cancer therapeutics.

Acknowledgments. This work was supported by a 2-Year Research Grant of Pusan National University.

References

1. Hsu, H.; Shu, H. B.; Pan, M. G.; Goeddel, D. V. *Cell* **1996**, *84*, 299.
2. Reed, J. C.; Doctor, K. S.; Godzik, A. *Sci. STKE* **2004**, 239:re9.
3. Stanger, B. Z.; Leder, P.; Lee, T. H.; Kim, E.; Seed, B. *Cell* **1995**, *81*, 513.
4. Song, H. Y.; Dunbar, J. D.; Donner, D. B. *J. Biol. Chem.* **1994**, *269*, 22492.
5. Boldin, M. P.; Mett, I. L.; Varfolomeev, E. E.; Chumakov, I.; Shemer-Avni, Y.; Camonis, J. H.; Wallach, D. *J. Biol. Chem*. **1995**, *270*, 387.
6. Hsu, H.; Xiong, J.; Goeddel, D. V. *Cell* **1995**, *81*, 495.
7. Chinnaiyan, A. M.; Rourke, K. O.; Tewari, M.; Dixit, V. M. *Cell* **1995**, *81*, 505.
8. Guan, Y. J.; Zhang, Z.; Yu, C.; Ma, L.; Hu, W.; Xu, L.; Gao, J. S.; Chung, C. S.; Wang, L.; Yang, Z. F.; Fast, L. D.; Chung, A. S.; Kim, M.; Ayala, A.; Zhuang, S.; Zheng, S.; Chin, Y. E. *J. Immunology* **2011**, *187*, 1289.
9. Guex, N.; Peitsch, M. C. *Electrophoresis* **1997**, *18*, 2714.
10. La skowski, R. A. *J. Appl. Cryst.* **1993**, *26*, 283.
11. Lin, S. C.; Lo, Y. C.; Wu, H. *Nature* **2010**, *465*, 885.
12. Park, H. H. *Apoptosis* **2011**, *16*, 209.
13. Ferrao, R.; Wu, H. *Curr. Opin. Struct. Biol.* **2012**, *22*, 241.